Comparison of algorithms of Time-lapse ERT inversion

MARIOS KARAOULIS[1], PANAGIOTIS TSOURLOS[2] and JUNG-HO KIM[3]

[1] Colorado School of Mines, Dept. of Geophysics, Golden, CO, USA.
[2] Aristotle University of Thessaloniki, Greece.
[3] Geoelectric Imaging Laboratory, Korea Institute of Geoscience and Mineral Resources, Daejeon, South Korea.

jungho@kigam.re.kr

Abstract

Electrical resistivity tomography (ERT) is often used for monitoring dynamic subsurface processes like remediation tests and geothermal processes. ERT imaging in a time-lapse mode ideally involves permanent electrode installations to maximize the repeatability of the measurements. It is a natural tool to complement standard geochemical or hydrogeological in situ sampling in wells, in providing spatio-temporal infomation that cannot be reached by direct sampling. Several single time step inversion algorithms have been proposed to model and invert DC/IP data, but as shown by many authors, inversion may be contaminated with inversion artifacts. Therefore, new inversion algorithms have been proposed, to reduce time related artifacts. The introduction of time into the data set can be achieved with the use of time-lapse tomographic algorithm and a variety of inversion strategies. In this work we will make a comparative study of some of some of the time-lapse inversion strategies.

Introduction

Electrical resistivity is sensitive to salinity, porosity, saturation, pore shape, temperature, clay content, and biological activity (e.g., WAXMAN and SMITS, 1968; REVIL et al., 1998; ATEKWANA et al., 2004). Variability in any of these parameters can have an influence on resistivity and can be monitored by time-lapse electrical resistivity tomography (TL-ERT). In the recent literature, TL-ERT has started to be a popular method to monitor dynamic processes occurring in the shallow subsurface (typically the first hundred meters, see LEGAZ et al., 2009, MÜLLER et al., 2010 and references therein). TL-ERT imaging, often involving permanent electrode installations, has proven to provide information complementary to in situ geochemical measurements. Applications of TL-ERT include monitoring of subsurface flow (e.g., DAILY et al., 1992; RAMIREZ et al., 1993; PARK, 1998; DAILY and RAMIREZ, 2000; NIMMER et al., 2007), characterization of solute transport (e.g., SLATER et al., 2002; KEMNA et al., 2002; SINGHA and GORELICK, 2005; LOOMS et al., 2008), saturation and temperature (LEGAZ et al., 2009), and mapping of salt-water intrusion in aquifers (e.g., NGUYEN et al., 2009; OGILVY et al., 2009) just to cite few applications.

A standard approach is to independently invert the measured data acquired at each monitoring step and to reconstruct time-lapse images (e.g. DAILY et al., 1992; RAMIREZ et al., 1993; BINLEY et al., 1996). As suggested by several researchers, the independent time-lapse inversion images may be strongly contaminated with inversion artifacts due to the presence of noise in the measurements and independent inversion errors. LABRECQUE and YOUNG (2001) and KIM et al. (2009) presented time-lapse algorithms to minimize those artifacts, but as shown by KARAOULIS et al. (2011), these

algorithmes may also suppress real changes in the complex resistivity due to the spurious effect associated with the selection of the time regularization parameter in the cost function.

Inversion

In this section, we descibe the different inversion strategies that can be applied to ERT data. We briefly report the single-time step inversion that is used in this work. In this work, **X** denotes the model, **d** denotes data and G the forward operator. It is important to notice that the main inversion equations remain the same no matter of the choice of 2D or 3D modeling.

Single time-step inversion

Consider the misfit vector **e** between the observed and calculated data that we need to minimize. Among different techniques we choose to minimize the L_2-norm of the following objective function *S*,

$$S = \|\boldsymbol{GX} - \boldsymbol{d}\|^2 + \lambda^2 \|\boldsymbol{CX}\|^2, \quad (1)$$

where λ denotes the tradeoff parameter that controls the model regularization and **C** is the second derivative of the model. The first term of the objective functions, ensures the convergence of the recovered model with respect to the observed data. The second part of the objection function, is introduced to stabilize the inversion algorithm, and produce smooth models (Constable et al., 1987).

The solution to this objective function is found either with an iterative Occam's update Equation (23),

$$\boldsymbol{X}_{i+1} = (\boldsymbol{J}^T\boldsymbol{J} + \lambda\, \boldsymbol{C}^T\boldsymbol{C})^{-1}\boldsymbol{J}^T(G(\boldsymbol{X}) - \boldsymbol{d} + \boldsymbol{J}^T\boldsymbol{X}) \quad (2)$$

By using each each date set seperatley,

Difference inversion

LABREQUE and YANG (2001) presented the difference inversion algorithm in an attempt to minimize possible inversion artifacts. They process time-lapse resistivity data by inverting for the differences between the background and subsequent data sets.

$$\Delta\boldsymbol{D} = (\boldsymbol{d}_t - \boldsymbol{d}_0) - (G(\boldsymbol{X}_t) - G(\boldsymbol{X}_0)), \quad (3)$$

$$\boldsymbol{X}_{i+1} = \boldsymbol{X}_i + (\boldsymbol{J}^T\boldsymbol{J} + \boldsymbol{C}^T\boldsymbol{\Lambda}\boldsymbol{C})^{-1}\boldsymbol{J}^T\Delta\boldsymbol{D}, \quad (4)$$

where the vectors $\boldsymbol{d}_0$ and $\boldsymbol{X}_0$ are the background data and model, while $\boldsymbol{d}_t$ and $\boldsymbol{X}_t$ are the data and model of the reference time-step *t*.

The difference inversion approach is the most popular for inverting time-lapse geoelectrical data as suggested by several published works (KEMNA el al., 2000 CASSIANI et al., 2007; LEROUX and DAHLIN, 2006; OLDENBORGER et al., 2007; TSOURLOS et al., 2008; DE FRANCO et al., 2009; MILLER et al., 2008; OGILVY et al., 2009).

4D inversion and 4D-ATC inversion

The 4D model as described by KIM et al. (2009) defines the subsurface as a combined space-time model which encompasses all space models during the entire monitoring period. The entire monitoring data are defined as a data vector in the space-time domain as well. The space-time model is assumed to change continuously along the time-axis, which allows the change of the subsurface material property distribution during the measurement of the geophysical datum.

Since both the data and the model are defined using space-time coordinates, the 4D-ATC algorithm is able to adopt regularization in both the time and space domains to stabilize the inversion. Consequently, the objective function S to be minimized by the inversion process can be expressed as follows (ZHANG et al., 2005; KIM et al., 2009),

$$S = \|\boldsymbol{e}^T\boldsymbol{e}\|^2 + \lambda\Psi + \alpha\Gamma, \quad (5)$$

where Ψ and Γ are the two regularization functions. The function Ψ is used for smoothness regularization in space and the function Γ is used for flatness regularization in time. The two parameters λ and α are the tradeoff parameters for controlling these two regularizations terms. Regarding the space-domain smoothness constraint, a second order differential operator is applied to the model perturbation vector. In the time domain, KIM *et al.* (2009) applied a first order differential operator to the model vector itself. This is based on the realistic assumption that the change of the material properties in the time domain is small compared to the space domain and the basic subsurface structure would remain the same throughout the entire monitoring period.

The time-domain tradeoff parameter is expressed either as a constant value α (**A**=α**I**) or as a diagonal matrix ***A*** (KARAOULIS *et al*., 2011a).

Minimizing the objective function (5) with respect to the model perturbation vector yields the following normal equations (Kim *et al.*, 2009),

$$\widehat{\boldsymbol{X}}^{k+1} = \widehat{\boldsymbol{X}}^k + d\widehat{\boldsymbol{X}} = + (\widehat{\boldsymbol{J}}^T\widehat{\boldsymbol{J}} + \widehat{\boldsymbol{C}}^T\widehat{\boldsymbol{\Lambda}}\,\widehat{\boldsymbol{C}} + \boldsymbol{M}^T\boldsymbol{A}\boldsymbol{M})^{-1}(\widehat{\boldsymbol{J}}^T\left(G\left(\widehat{\boldsymbol{X}}^k\right) - \widehat{\boldsymbol{D}}\right) - \boldsymbol{M}^T\boldsymbol{A}\boldsymbol{M}\widehat{\boldsymbol{X}}^k). \quad (6)$$

where **M** is a square matrix.

Synthetic test

Modeled data obtained for 5 different time steps representing a hypothetical time-lapse induced polarization change are depicted in Figures 1. A total of 225 surface electrodes were used to obtain surface dipole-dipole data (inter-electrode spacing *a*=1 with maximum intra-dipole spacing *dn* = 7) with 945 measurements for each time-step. The background model had an resistivity of 10 Ohm m.

Figure 2 and 3 shows the difference images, when comparing the independent inversion, the difference inversion, and the 4D/4D-ATC inversion. We can observer that the difference inversion mimics better the actual change than the independent inversion, but the amplitude is smallest than the actual one. Besides that, the area of the actual change is shown more extensive than the modeled one, indication of artifacts. 4D/4D-ATC inversion shows the actual change best, both in position and actual amplitude. Figure 4 shows the model RMS error, where the 4D/4D-ATC invasion achieves the smallest misfit, indication that the modeled changes are closer to the actual one.

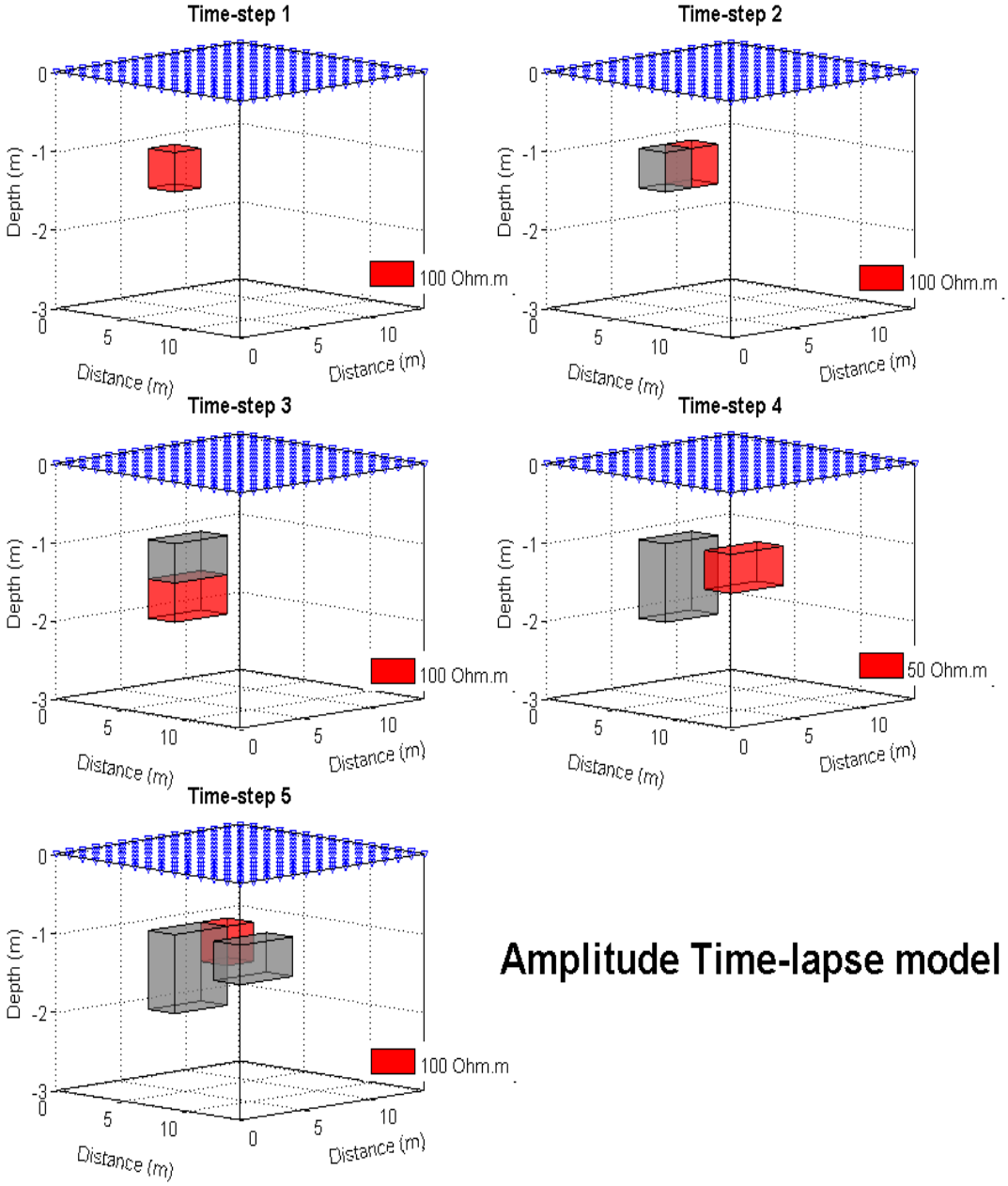

Fig. 1: The 4D resistivity model used in this work showing the changes in amplitude through time (five time-steps). The grey cubes denote the synthetic model used in the previous time-step. The red cubes show the change in that time-step with respect to the previous time-steps. The background model has a constant resistivity amplitude of 10 Ωm.

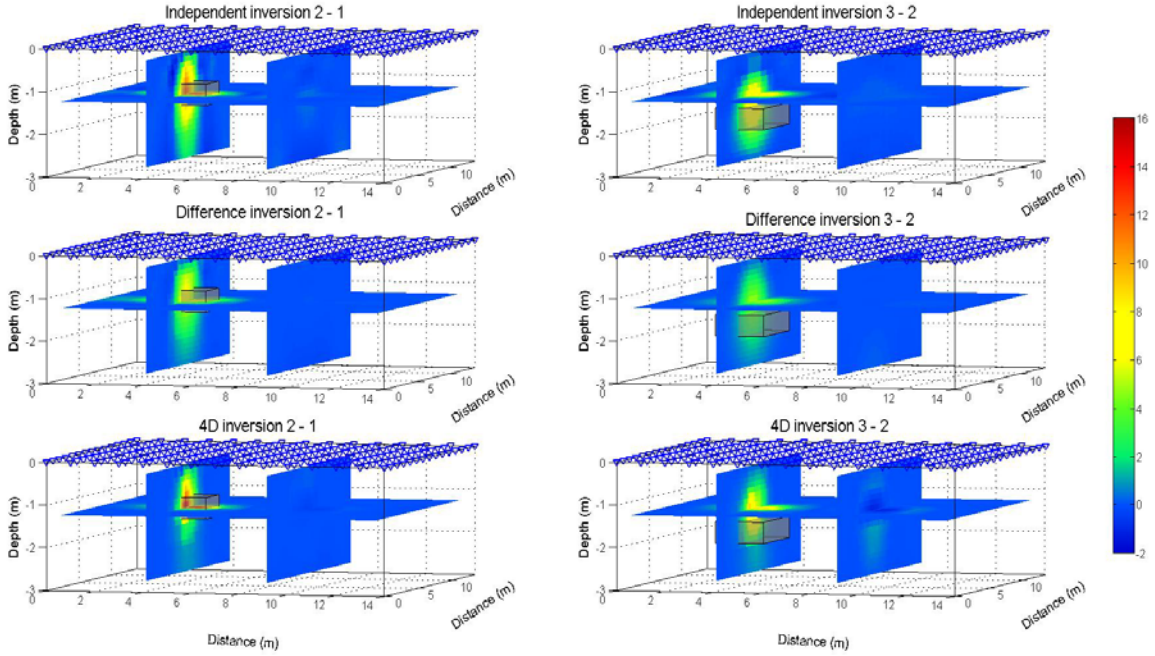

Fig. 2: Difference Images when using three different inversion algorithms for time steps 2-1 and 3-2. Grey cube denotes the area of the modeled change.

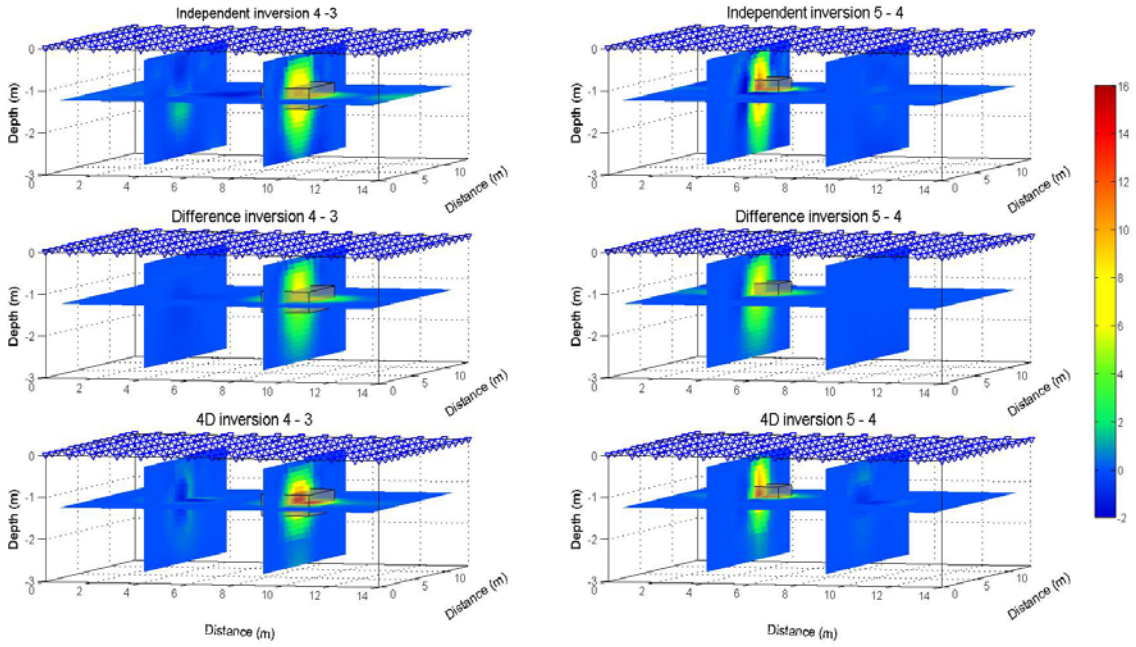

Fig. 3: Difference Images when using three different inversion algorithms for time steps 4-3 and 5-4. Grey cube denotes the area of the modeled change.

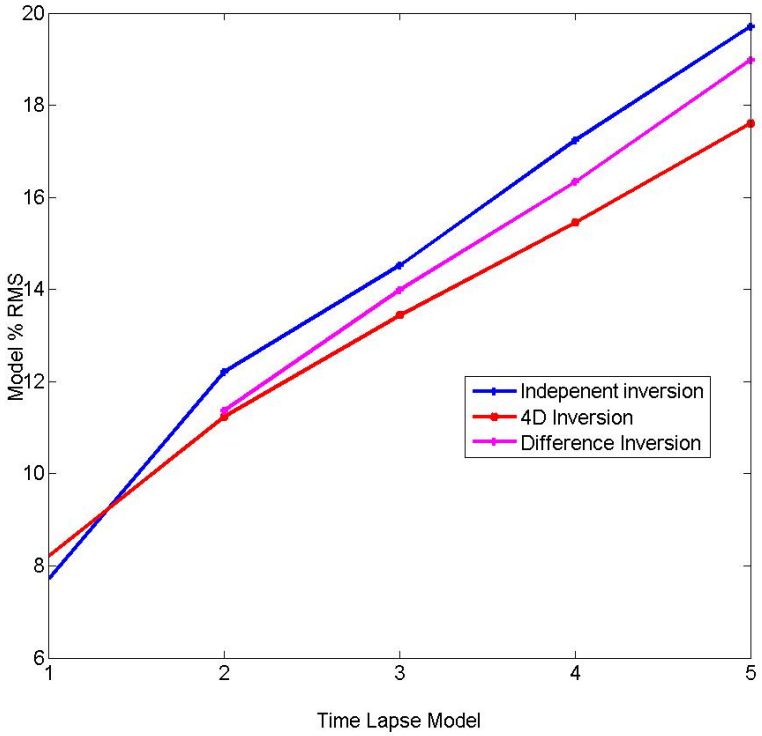

Fig. 4: The % model misfit from all tested algorithm. The smallest model rms error was observed by using the 4D/4D-ATC algorithm.

Conclusions

Independent inversion, as shown from numerical and real data, produces the most artifacts, which in some cases can lead to a false interpretation of the monitoring data. Difference inversion, seems to reduce those artifacts, but it does not eliminated them. 4D and 4D-ATC techniques have the least artifacts and produce the most realistic images.

References

BINLEY, A., HENRY-POULTER, S. and SHAW, B., 1996: Examination of solute transport in an undisturbed soil column using electrical resistance tomography. – Water Resources Research, **32**, 763–769.

CASSIANI, G., BINLEY, A. and FERRÉ, T.P.A., 2007: Unsaturated zone processes. – Applied Hydrogeophysics, **71**, 75-116.

CONSTABLE, S., PARKER, R. and CONSTABLE, C., 1987: Occam's inversion: A practical algorithm for generating smooth models from electromagnetic sounding data. – Geophysics, **52**, 289-300.

DAILY, W., RAMIREZ, A., LABRECQUE, D. & NITAO, J., 1992: Electrical resistivity tomography of vadose water movement. – Water Resources Research, **28**, 1429-1442.

DAILY, W. and RAMIREZ, A.L., 2000: Electrical imaging of engineered hydraulic barriers. – Geophysics, **65**, 83-94.

KARAOULIS, M., KIM, J.-H. and TSOURLOS, P.I., 2011: 4D Active Time Constrained Inversion. – Journal of Applied Geophysics, **73**, 25-34.

KEMNA, A., BINLEY, A., RAMIREZ, A. and DAILY, W., 2000: Complex resistivity tomography for environmental applications. – Chemical Engineering Journal, **77**, 11–18.

KIM, J.-H., YI, M.J., PARK, S.G. and KIM, J.G., 2009: 4-D inversion of DC resistivity monitoring data acquired over a dynamically changing earth model. – Journal of Applied Geophysics, **68**(4), 522-532.

LABRECQUE, D.J. and YANG, X., 2001: Difference inversion of ERT data: a fast inversion method for 3-D in situ monitoring. – Journal of Environmental and Engineering Geophysics, **5**, 83-90.

LEGAZ, A., VANDEMEULEBROUCK, J., REVIL, A., KEMNA, A., HURST, A.W., REEVES, R. and PAPASIN, R., 2009: Acase study of resistivity and self-potential signatures of hydrothermal instabilities, Inferno Crater Lake, Waimangu, New Zealand. – Geophysical Research Letters, **36**, L12306, doi: 10.1029/2009GL037573.

LEROUX, V. and DAHLIN, T., 2006: Time-lapse resistivity investigations for imaging saltwater transport in glaciofluvial deposits, Environmental Geology, **49**(3), 347-358.

LOOMS, M.C., JENSEN, K.H., BINLEY, A. and NIELSEN, L., 2008: Monitoring unsaturated flowand transport using cross-borehole geophysical methods. – Vadose Zone Journal, **7**, 227–237.

MILLER, C.R., ROUTH, P.S., BROSTEN, T.R., and MCNAMARA, J.P., 2008: Application of time-lapse ERT imaging to watershed characterization. – Geophysics, **73**, G7-G17.

MÜLLER, K., VANDERBORGHT, J., ENGLERT, A., KEMNA, A., HUISMAN, J.A., RINGS, J. and VEREECKEN, H., 2010: Imaging and characterization of solute transport during two tracer tests in a shallow aquifer using electrical resistivity tomography and multilevel groundwater samplers. Water Resources Research, **46**, W03502, doi: 10.1029/2008WR00.

NGUYEN, F., KEMNA, A., ANTONSSON, A., ENGESGAARD, P., KURAS, O., OGILVY, R., GISBERT, J., JORRETO, S. and PULIDO-BOSSCH, A., 2009: Characterization of seawater intrusion using 2D electrical imaging. – Near-Surface Geophysics, **7**(5-6), 377-390.

NIMMER, R.E., OSIENSKY, J.L., BINLEY, A.M., SPRENKE, K.F. and WILLIAMS, B.C., 2007: Electrical resistivity imaging of conductive plume dilution in fractured rock. – Hydrogeology Journal, **5**, 877-890.

OGILVY, R D., KURAS, O., MELDRUM, P I., WILKINSON, P B., CHAMBERS, J. E., SEN, M., GISBERT, J., JORRETO, S., FRANCES, I., PULIDO-BOSCH, A. and TSOURLOS, P., 2009: Automated time-Lapse Electrical Resistivity Tomography (ALERT) for monitoring Coastal Aquifers. – Near Surface Geophysics, **7**(5-6), 367-375.

OLDENBORGER, G.A., KNOLL, M.D., ROUTH, P.S. and LABRECQUE, D.J., 2007: Time-lapse ERT monitoring of an injection/withdrawal experiment in a shallow unconfined aquifer. – Geophysics, **72**(4), F177-F187.

PARK, S., 1998: Fluid migration in the vadose zone from 3-D inversion of resistivity monitoring data. – Geophysics, **63**(1), 41-51.

RAMIREZ, A., DAILY, W., LABRECQUE, D.J., OWEN, E. and CHESNUT, D., 1993: Monitoring an underground steam injection process using electrical resistance tomography. – Water Resources Research, **29**, 73-87.

SINGHA, K. and GORELICK, S.M., 2005: Saline tracer visualized with electrical resistivity tomography: field scale spatial moment analysis. – Water Resour. Res., **41**, W05023, doi: 10.1029/2004WR003460.

SLATER, L., BINLEY, A.M., VERSTEEG, R., CASSIANI, G., BIRKEN, R. and SANDLEBERG, S., 2002: A 3D ERT study of solute transport in a large experimental tank. – Journal of Applied Geophysics, **49**(4), 211–229.

ZHANG, Y., GHODRATI, A., BROOKS, D.H., 2005: An analytical comparison of three spatiotemporal regularization methods for dynamic linear inverse problems in a common statistical framework. – Inverse Problems, **21**, 357-382.